DOI: 10.1021/ma101145r

Macromolecules
ARTICLE

Shape Memory Behavior of Side-Chain Liquid Crystalline Polymer Networks Triggered by Dual Transition Temperatures

Suk-kyun Ahn,[†] Prashant Deshmukh,[‡] and Rajeswari M. Kasi*[,†,‡]

[†]*Polymer Program, The Institute of Materials Science, University of Connecticut, Storrs, Connecticut 06269, and* [‡]*Department of Chemistry, University of Connecticut, Storrs, Connecticut 06269*

Received May 22, 2010; Revised Manuscript Received July 24, 2010

ABSTRACT: We report synthesis and characterization of a new class of side-chain liquid crystalline random terpolymers (SCLCP), its cross-linked network (SCLCN), and the corresponding shape memory properties. The SCLCP comprising three monomers, 5-{15-(cholesteryloxycarbonyl)-pentadecyloxycarbonyl}-bicyclo[2.2.1]hept-2-ene (NBCh15), 5-(acryloyl butoxycarbonyl)-bicyclo[2.2.1]hept-2-ene (NBBA), and poly(ethylene glycol) functionalized norbornene (NBPEG), is synthesized by ring-opening metathesis polymerization (ROMP) using Grubbs catalyst second generation, resulting in a random terpolymer. Each monomer provides a specific function in the terpolymer: (1) NBCh15 affords liquid crystalline properties, (2) NBBA is a cross-linkable unit, and (3) NBPEG acts as an internal plasticizer. The mesomorphic structure of the terpolymer investigated by X-ray diffraction (XRD) exhibits highly interdigitated smectic A (SmA) mesophase comprising cholesteryl ester mesogens. The acrylate end group in the NBBA undergoes cross-linking by curing at 120 °C, resulting in the SCLCN. Optimal cross-linking conditions are determined by monitoring gel fraction produced from different curing times. Thermal transitions including glass transition temperature (T_g) and clearing temperature (T_{cl}) before and after cross-linking are analyzed by differential scanning calorimetry (DSC). Linear viscoelastic properties of the SCLCN reveal three different relaxations associated with dynamic soft elasticity as well as T_g and T_{cl}. One-way shape memory cycles (1W-SMCs) of the SCLCN are programmed using (1) T_g, (2) T_{cl}, and (3) combined (T_g and T_{cl}) as a shape memory transition temperature (T_{trans}). The T_g-based SMCs exhibits excellent shape fixing (> 97%) and shape recovery ratio (> 96%) with large strain (> 150%). In the T_{cl}-based SMCs, the cooling induced elongation of strain is observed due to the development of interdigitated SmA mesophase. The shape fixing by interdigitated SmA is achieved during the T_{cl}-based SMCs unlike conventional shape fixing methods such as vitrification or crystallization. If both T_g and T_{cl} serve as T_{trans} for SMCs, the permanent shape is restored by two stages of shape recovery around T_g and T_{cl}. The dual T_{trans} (T_g and T_{cl}) inherent in this SCLCN allows for creating different types of SMCs and for the memorization of shape at two different temperature windows, thereby, programmed shapes by different mechanism would be recovered in a more precise manner.

1. Introduction

Shape memory polymers (SMPs) are an exciting class of stimuli-responsive materials, which have the capability to switch from temporary to permanent shape when exposed to stimuli such as heat,[1−6] light,[7−10] pH,[11] moisture[12] or magnetic field.[13] Applications of these materials include intelligent biomedical devices,[14−17] controlled drug release,[18−20] tissue engineering scaffolds,[21,22] smart fabrics,[23] fasteners,[24] sensors,[25] and soft lithography.[26]

The majority of current SMPs are thermally activated through a transition temperature (T_{trans}), which can be a glass transition temperature (T_g),[27−32] melting temperature (T_m, in semicrystalline polymers)[33−35] or liquid crystalline clearing temperature (T_{cl}, in liquid crystalline polymers).[26,36,37] The process of thermo-responsive SMPs typically includes (i) programming process by deformation of shape with an external stress at a temperature above T_{trans}, followed by fixation of shape by cooling to a temperature below T_{trans} and (ii) recovery process by reheating the sample above T_{trans} at the stress-free state. Physical or chemical cross-links are required to prevent polymer chains from disentangling and slipping off each other during deformation, and these cross-links determine permanent shape.[4,38]

*Corresponding author. E-mail: kasi@ims.uconn.edu.

When the deformed polymer is cooled below T_{trans}, the mobility of the polymer chain is constrained by physical cross-links such as vitrification at a temperature below T_g or crystallization at a temperature below T_m. As a result, the temporary shape can be fixed by these physical cross-links. Physical cross-links also prevent the temporary shape from returning to the permanent shape when external stress is removed. Chain configurations in a temporary shape retains less entropy due to stretching, which spontaneously maximizes the entropy during reheating by adopting Gaussian configuration, presented in its permanent shape and shown to be the recovery process.[39]

SMPs can be divided into two types, one-way (1W) or two-way (2W), which differ in the memory capability of their shapes.[4,36] The one-way shape memory polymers (1W-SMPs) only remember their permanent shapes. Therefore, the deformation process is driven by an external stress, and only the recovery process is spontaneous. However, two-way shape memory polymers (2W-SMPs) can remember both permanent and temporary shapes, under constant nonzero stress, so that both shapes can be reversibly actuated upon heating and cooling, respectively. Different temporary shapes can be obtained in the 1W-SMPs during the programming process, whereas, thermally reversible actuation can be realized through the 2W-SMPs.

Liquid crystalline elastomers (LCEs) or networks (LCNs) are used for thermo-responsive applications including SMPs[2,6,26,36,37,40,41]

 Published on Web 08/06/2010

Scheme 1. Synthesis of Terpolymer (TP15) by Ring-Opening Metathesis Polymerization (ROMP) Using Grubbs Catalyst Second Generation at Room Temperature[a]

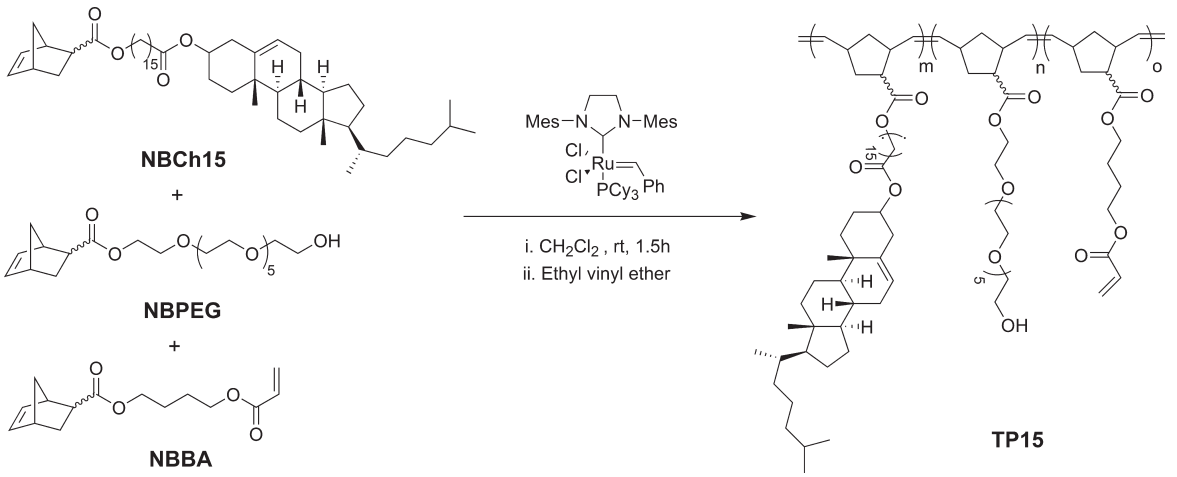

[a] The *endo* and *exo* isomers are represented as wavy lines.

and artificial muscles.[42−47] In nematic type LCEs or LCNs, conformational change from the extended prolate in the nematic state to the contracted sphere in the isotropic state or vice versa is a driving force for the reversible extension/contraction under influence of external thermal stimulus but constant stress.[43] These large extentions/contractions result in mechanical work that can be harnessed for actuators and artificial muscle applications. Smectic type LCEs or LCNs have received less attention for thermo-responsive applications, however, these materials show interesting shape memory effect (SME). Mather and co-workers have prepared polysiloxane-based main-chain LCEs that exhibit unique smectic C (SmC) mesophase which show exceptional SME and actuator behavior.[26,37] Finkelmann and co-workers have performed seminal work on polysiloxane comprising both side-chain smectic A (SmA) and chiral smectic C (SmC*) elastomers that show reversible uniaxial or biaxial contraction/elongation, respectively, upon application of thermal stimulus.[41,48] However, the detailed thermomechanical analysis in terms of SME have not been examined in these polymers.

Recently, we have reported a facile method to prepare polynorbornene bearing cholesteryl side-chains (PNBCh-*n*), where *n* is the length of the methylene spacer.[49] These polymers exhibit primarily SmA mesophases, which depending on the length of the methylene spacer, could form bilayer and interdigitated SmA mesophases. These polymers show T_g and T_{cl} that can be tailored by choice of the spacer length. However, SME using T_g or T_{cl} is not possible using these polymers due to absence of cross-linked network. It is important to introduce cross-links to produce SME either by cross-linking of polynorbornene backbone[50] or incorporation of comonomers that can be used to produce networks by photo- or thermal cross-linking. We decided to incorporate two other comonomers such as poly(ethylene glycol) functionalized norbornene (NBPEG) and 5-(acryloyl butoxycarbonyl)-bicyclo[2.2.1]hept-2-ene (NBBA) along with 5-{15-(cholesteryloxycarbonyl)-pentadecyloxycarbonyl}-bicyclo[2.2.1]hept-2-ene (NBCh15)[49] to tune physical and mechanical properties of the resulting terpolymer (TP15) precisely by changing composition of the monomers. Each monomer provides specific function in the TP15: (1) NBCh15 affords liquid crystalline properties, (2) NBPEG acts as an internal plasticizer, and (3) NBBA is a cross-linkable unit.

In this work, we describe the synthesis and characterization of the new terpolymer composition and investigate detailed 1W-SME using the TP15-based side-chain liquid crystalline network (SCLCN) which exhibits highly interdigitated SmA mesophase.

Table 1. Preparation of Terpolymer (TP15)

	mol %[a]					
polymer	NBCh15	NBPEG	NBBA	yield (%)	M_n (g/mol)[b]	PDI[b]
TP15[c]	80.5 (79.0)	15.5 (15.3)	4.0 (5.7)	89.4	97 482	1.54
PNBCh15[d]	100			75.2	59 228	1.42

[a] Mol % is calculated from ^{1}H NMR, where peaks at 4.6, 3.6, and 5.8 ppm are used to quantify composition of NBCh15, NBPEG, and NBBA, respectively. Values in parentheses indicate concentration of monomer in feed. [b] Polystyrene standards are used for constructing GPC calibration curves. [c] Polymerization is conducted using mole ratio of [NBCh15]/[I]: [NBPEG]/[I]: [NBBA]/[I] = 146.3: 28.4: 10.6, where I represents initiator. [d] Preparation of homopolymer (PNBCh15) is reported in our publication.[49]

To the best of our knowledge, this SCLCN is the first example of SmA-based SMPs containing inherent dual T_{trans} (lower T_g and higher T_{cl}) within a single system, which can be utilized to program different SMEs. We will be able to harness unique properties of SmA networks systems that have not been exploited before including (1) the extent of interdigitation in the SmA layers which will impact on the final shape memory properties and (2) fluidity within the SmA layers affording flexibility akin to biological membranes.[51,52] This terpolymer system is a promising candidate for in vitro tissue engineering and other biomedical applications due to high thermodynamic affinity of the cell membranes for cholesteryl moieties,[53−55] low cytotoxicity of polynorbornenes[56] and biocompatibility of PEG.[57]

2. Results and Discussion

2.1. Synthesis of Monomers and Terpolymer. Monomers, NBCh15,[49] NBPEG,[58,59] and NBBA,[60] are synthesized according to modified literature procedures and their composition and purity are evaluated. ^{1}H NMR spectra and peak assignments of NBPEG and NBBA and a mass spectrum of NBPEG are presented in Supporting Information, Figures S1, S2, and S3, respectively.

Ring-opening metathesis polymerization (ROMP) is carried out using NBCh15, NBPEG, and NBBA with Grubbs catalyst second generation in CH_2Cl_2, Scheme 1 and Table 1. The premade monomers and catalyst solutions are separately purged under nitrogen for 15 min each, and then two solutions are combined together. Polymerization is allowed to proceed for 1.5 h at room temperature and terminated by adding ethyl vinyl ether (EVE). The resulting polymer is precipitated in methanol, filtered, followed by drying overnight under vacuum at room temperature. Several terpolymer

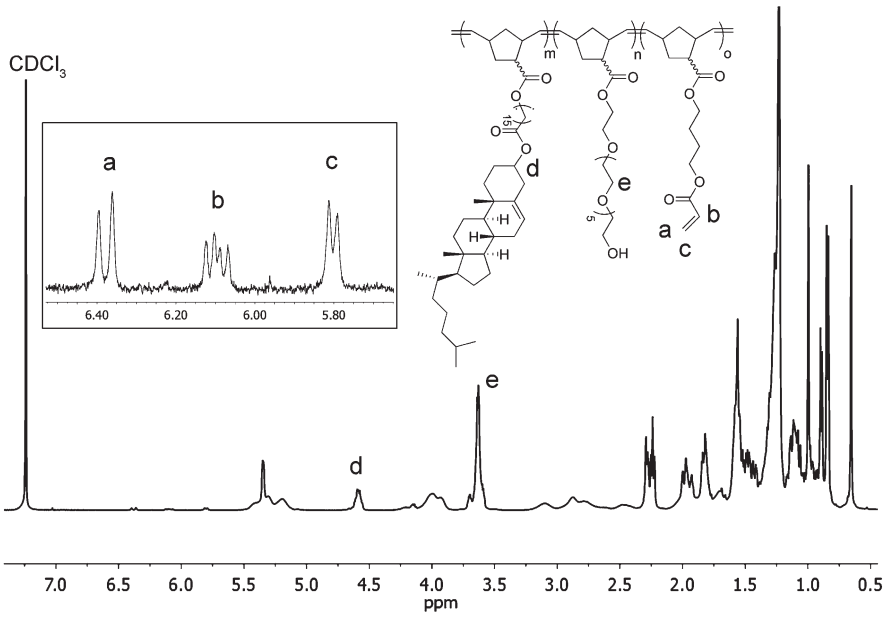

Figure 1. ^{1}H NMR of TP15 in $CDCl_3$ at room temperature. The expanded vinyl end-group region of NBBA is shown in the inset.

Table 2. Transition Temperatures

polymer	T_g (°C)[a]	T_{cl} (°C)[a]	ΔH (J/g)[a]
TP15[b]	23.0	104.1	5.45
XL-TP15[c]	22.5	103.5	5.36
PNBCh15[d]	35.6	104.6	5.14
PNBBA[e]	−9.7		
PNBPEG[e]	−48.7		

[a] All transitions values are determined from DSC second heating cycle with a rate of 10 °C/min. [b] TP15 is partially cross-linked after the first heating cycle due to thermal cross-linking. [c] The sample is thermally cross-linked by annealing at 120 °C for 48 h under vacuum and its gel fraction is 89.0%. [d] The thermal properties of homopolymer of NBCh15 (PNBCh15) are reported in our previous publication.[49] [e] PNBBA and PNBPEG represent homopolymer of NBBA and NBPEG, respectively.

compositions are synthesized (Table S1), however, in this paper we will focus on the synthesis and characterization of one terpolymer (TP15) and investigate its SME.

A representative ^{1}H NMR spectrum of TP15 is shown in Figure 1. The peaks **a**, **b**, **c** at 5.8−6.4 ppm represent three protons in the vinyl group of NBBA, and peak **d** at 4.6 ppm corresponds to one proton next to oxygen in the cholesteryl group of NBCh15. The peak, **e**, corresponds to 26 protons in NBPEG. Using the integration of these peaks and corresponding number of protons, the mole ratio of the monomers in TP15 is determined, and this agrees well with feed ratio listed in Table 1. The conversion from monomer to polymer is clean and quantitative as seen from ^{1}H NMR of TP15.

2.2. Thermal and Linear Viscoelastic Properties. Differential scanning calorimetry (DSC) is used to determine transition temperatures of polymers and their associated enthalpy (ΔH), Table 2. The uncross-linked terpolymer (TP15) is initially heated to 150 °C, cooled to −50 °C and reheated to 150 °C. The first heating cycle is used to eliminate the thermal history of the sample and inevitably allows thermal cross-linking, resulting in partially cross-linked TP15. Nevertheless, the T_g of TP15 in the second heating cycle is ∼10 °C lower than the T_g of its homopolymer counterpart (PNBCh15) due to the incorporation of more flexible NBPEG and NBBA units in the TP15. The T_{cl} of TP15 and PNBCh15 are approximately 104 °C and the corresponding ΔH values are also similar. This suggests that there is no significant

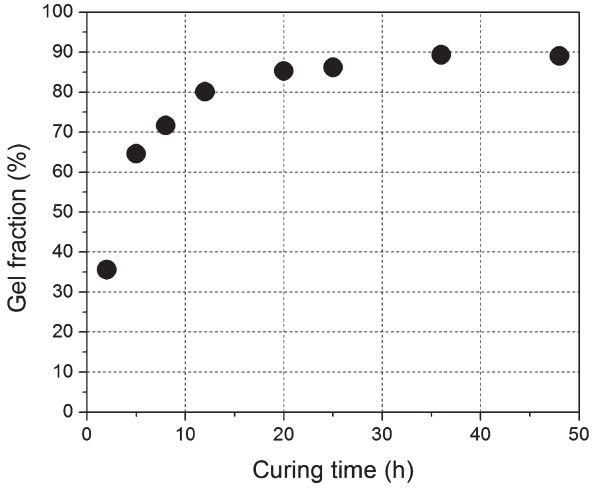

Figure 2. Gel fraction as a function of a curing time. Each gel fraction value is determined by the ratio between mass of XL-TP15 film before and after extraction in THF.

dilution effect on the liquid crystalline (LC) ordering in the terpolymeric system despite the introduction of ∼20 mol % of other functional groups (NBPEG and NBBA) to the system.

Physical or chemical cross-links are essential for SMPs since the permanent shape is attained during the cross-linking process.[4] Cross-linking also prevents the polymers from de-entangling and allows improved shape recovery. In TP15, the acrylate end groups of NBBA form chemical cross-links simply by heating at 120 °C in the absence of initiators (thermal curing).[61,62] Quantitative conversion to terpolymer network (XL-TP15) is attained by thermally curing TP15 for 48 h at 120 °C under vacuum. Gel fraction values determined from ratio between mass of XL-TP15 before and after extraction at different curing time are shown in Figure 2. The gel fraction increases rapidly to 80.1% after 12 h curing and slowly reaches to maximum value 89.0% after 48 h curing, which suggests 48 h is the optimal time for the thermal cross-linking. Both T_{cl} and its associated enthalpy of XL-TP15 after 48 h curing are slightly lower than the

values of the TP15 as determined from DSC (Table 2). The reduction in T_{cl} and enthalpy is attributed to the hindrance in liquid crystalline ordering by the formation of cross-links similar to the cross-linked semicrystalline polymers.[35]

DSC thermogram and linear viscoelastic properties obtained by dynamic mechanical analysis (DMA) of XL-TP15 agree well with each other, Figure 3. As mentioned previously, the TP15 exhibits distinct a T_g and a T_{cl} at 22.5 and 103.5 °C, respectively, Figure 3a. As shown in Figure 3b, at temperatures below T_g, XL-TP15 reveals typical storage modulus (E') of polymers (10^3 MPa), and no significant changes in loss modulus (E'') and tan δ are observed. As temperature approaches T_g, the E' decreases dramatically, and characteristic peaks associated with T_g are observed from both E'' and tan δ, respectively. In particular, the tan δ trace reveals a secondary peak at 60 °C, while no noticeable changes are detected in the E′ or E″ as well as the DSC thermogram at this temperature. The secondary peak in tan δ is attributed to the dynamic soft elasticity or a polydomain−monodomain (PM) transition.[36] Since the XL-TP15 is cross-linked without preferential alignment, the directors of the LC domains in the XL-TP15 are expected to be randomly distributed (polydomain). However, when the temperature approaches 60 °C, the overall directors of LC polydomain gain sufficient mobility to reorient along the loading direction, resulting in a monodomain like structure of the XL-TP15. During this reorientation process, the initial stored energy in the XL-TP15 is dissipated, which is reflected as an additional peak at 60 °C in tan δ. Finally, both E' and E'' exhibits secondary drop at T_{cl} and E' reaches to a plateau indicating cross-linked networks of the XL-TP15. The tan δ exhibits a weak and broad peak at T_{cl} and vanishes as the temperature further increases.

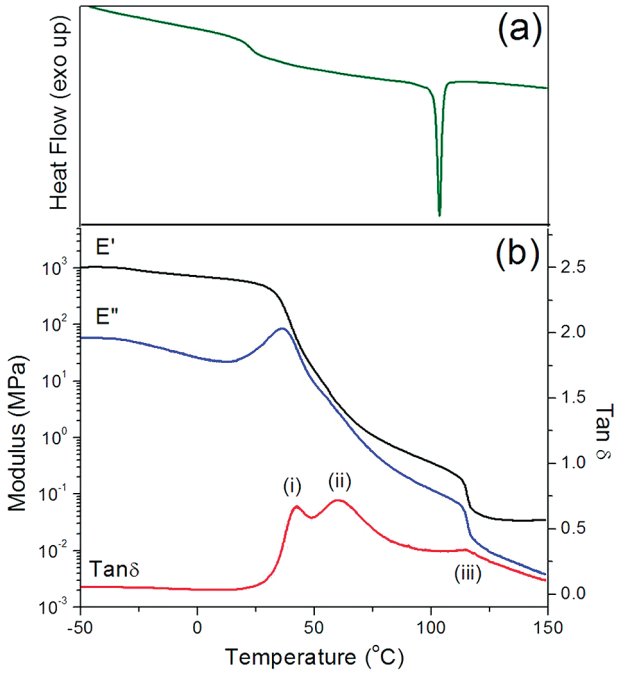

Figure 3. Thermal and linear viscoelastic properties of XL-TP15: (a) First heating DSC thermogram (green) with heating rate of 10 °C/min recorded after cross-linking at 120 °C for 12 h exhibits T_g and T_{cl} and (b) Tensile storage modulus (E', black), loss modulus (E'', blue) and tan δ (red) is measured by DMA. Here, tan δ reveals three characteristic peaks, where peak i at 42 °C represents a relaxation of polymer chains associated with T_g, peak ii at 60 °C is attributed to the dynamic soft elasticity, and a broad peak (peak iii) at 115 °C is associated with the molecular relaxation at T_{cl}.

2.3. Microstructural Analysis. To determine microstructure of the LC mesophase in TP15, the 1D and 2D wide-angle X-ray (WAXD) experiments are conducted. Figure 4a shows 1D-WAXD results from TP15 film prepared by compression molding. The first order reflection peak, d_1 (4.79 nm), corresponds to a distance between repeated smectic layers, while d_2 (2.43 nm) and d_3 (1.63 nm) are second and third order reflection peaks of d_1 indicating higher orders of smectic layers. The stronger intensity of d_2 compared to d_1 observed in the TP15 is probably due to the high electron density profile at the half of the interdigitated SmA layer in which PEG and cholesteryl side-chains overlap. However, the details of the electron density profile have not been investigated in this publication. In the 2D-WAXD shown in Figure 4b, the sample exhibits anisotropy due to the uniaxial compression, which induces strong alignment of smectic layers only in the direction parallel to the compression (y-direction),

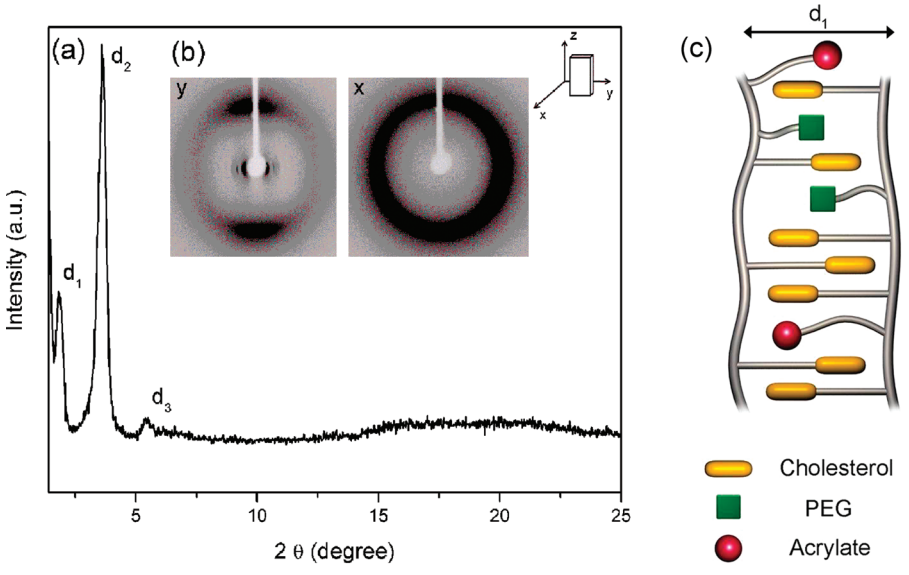

Figure 4. WAXD patterns at room temperature for the uncross-linked terpolymer (TP15) film prepared by compression molding at 50 °C: (a) 1D WAXD pattern, (b) 2D WAXD patterns in which X-ray beam is directed along the y- and x-directions as shown, and (c) schematic illustration of molecular packing structure of TP15 in the y-direction.

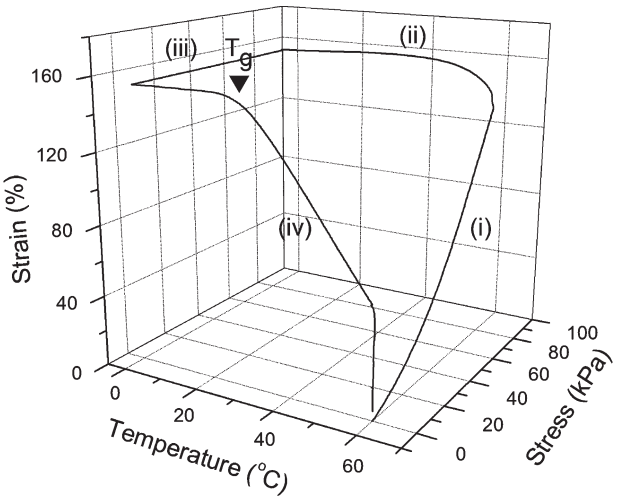

Figure 5. 3D diagram of T_g-based one-way shape memory cycle (1W-SMC, 5th cycle) for XL-TP15: (i) deformation, (ii) cooling, (iii) unloading and shape fixing, and (iv) recovery.

while the squeezing flow generated during compression above T_g eliminates smectic ordering in the direction normal to the compression (x-direction). Therefore, the TP15 film prepared by compression molding exhibits homeotropic alignment. When the film is exposed parallel to the X-ray beam (y-direction), the strong diffraction peaks on the equator corresponding to the distance of smectic layers and broad scatterings on the meridian for intermesogen spacing within smectic layers are observed, which suggests the director of smectic layer is aligned perpendicular to the polymer main-chain. The diffraction pattern in 2D-WAXD is a characteristic of smectic A (SmA) mesophase. The d_1 reflection peak is not detectable in the 2D-WAXD due to instrumental limitation.

The energy minimized bilayer model of the PNBCh15, an analogue of TP15, is constructed using Materials Studio 4.4 (Accelrys), Figure S4, Supporting Information. The d-spacing obtained from this bilayer model is 8.6 nm which is nearly twice the value for d-spacing (4.79 nm) measured from the WAXD results of TP15. Therefore, a highly interdigitated SmA layers is expected in the TP15 as illustrated in Figure 4c. The WAXD result of XL-TP15 is similar to TP15, indicating the preservation of SmA order after cross-linking.

2.4. Shape Memory Properties. Quantitative shape memory properties including shape fixity (R_f) and shape recovery (R_r) are investigated by cyclic thermomechanical analysis using DMA. XL-TP15 exhibits three different phases from glassy to SmA to isotropic phase upon heating, and the corresponding two distinct transition temperatures are T_g at 22.5 °C and T_{cl} at 103.5 °C. Three independent shape memory cycles (SMCs) are programmed using T_g and T_{cl} as the shape memory transition temperature (T_{trans}) of SMCs. The analyses of SMCs are divided into four different categories: (i) T_g-based SMCs whose temperature range (0−60 °C) includes glassy and SmA phase of XL-TP15 to assess shape fixity by vitrification, (ii) T_{cl}-based SMCs whose temperature range (60−120 °C) includes SmA and isotropic phase of XL-TP15 to evaluate shape fixity and recovery by LC ordering, (iii) ($T_g + T_{cl}$)-based SMCs whose temperature range (0−120 °C) includes glassy, SmA, and isotropic phase to understand the combined influences of T_g and T_{cl} during SMCs, and (iv) comparison of shape recovery events for different SMCs.

(*i*). *T_g Based SMCs.* T_g-based SMCs of XL-TP15 is investigated by monitoring strain responses as a function of temperature (0−60 °C) and stress (3.5−87.8 kPa). Five consecutive SMCs are performed and a representative 3D plot based on the fifth cycle of T_g-based SMCs for XL-TP15 is described in Figure 5. This SMC consists of four consecutive segments. In the first step, the sample is deformed at a temperature above T_g (60 °C), resulting in a linear increase of strain (deformation). In the second step, the sample is cooled below T_g (0 °C) under constant stress to freeze the extended strain (cooling). While cooling the sample, strain initially increases due to the creep response of the material under constant stress and then plateaus as the sample vitrifies below T_g. In the third step, the applied stress is reduced to the preload value (3.5 kPa) at 0 °C, and the strain remains constant (unloading and shape fixing). In the fourth step, the sample is reheated to 60 °C and the extended strain starts to recover when the temperature exceeds T_g of the sample (recovery). The temperature is held at 60 °C for additional 40 min to recover any residual strain (recovery).

Table 3. Strain, Shape Fixity (R_f), and Shape Recovery (R_r) of XL-TP15 in T_g-Based SMCs[a]

cycle no.	strain (%)	R_f (%)	$R_r(1)$[b] (%)	$R_r(2)$[c] (%)
1	139.7	97.5	53.6	87.5
2	144.0	97.4	60.7	95.4
3	149.8	97.4	62.8	96.9
4	155.8	97.6	63.3	96.5
5	158.2	97.5	63.6	96.6

[a] Conditions during SMCs: Temperature (0−60 °C) and applied stress (87.8 kPa). [b] $R_r(1)$ is a shape recovery at 60 °C. [c] $R_r(2)$ is a shape recovery at 60 °C after 40 min of isothermal step.

The strain, R_f, and R_r of XL-TP15 during T_g-based SMCs are listed in Table 3. The R_f, which quantifies the ability to fix a mechanical deformation, and the R_r, which quantifies the ability to restore the mechanical deformation, are calculated using the following equations:[3,63]

$$R_f(\%) = \frac{\varepsilon_u(N)}{\varepsilon_m(N)} \times 100,$$

$$R_r(\%) = \frac{\varepsilon_m(N) - \varepsilon_p(N)}{\varepsilon_m(N) - \varepsilon_p(N-1)} \times 100$$

where ε_u is the strain after unloading the applied force, ε_m is the resulting maximum strain by deformation, ε_p is the strain after completion of recovery step, and N is the number of cycles.

T_g-based SMCs for XL-TP15 exhibits excellent shape fixity and shape recovery. R_f is higher than 97% and preserved during SMCs, which indicates vitrification in the glassy state (0 °C) is efficient in freezing chain mobility and storing elastic energy. When the sample is reheated to 60 °C in the recovery step, only a modest R_r value ($R_r(1)$ = 63.6%, fifth cycle) is attained and high R_r value ($R_r(2)$ = 96.6%, fifth cycle) is finally achieved after isothermally holding the sample at 60 °C for additional 40 min. The slow shape recovery may be attributed to the slow relaxation behavior of polymeric chain at transition from glassy to soft SmA mesophase. XL-TP15 shows increase of R_r at higher cycle number, and the relatively poor performance on shape recovery seen in the first few cycles has been observed before.[4] The reorganization of polydomain SmA layers upon deformation along the loading direction during SMCs also contributes to increased R_r up to 96% at higher cycle number.

The presence of network structure is crucial to achieve consistent SMCs and high shape recovery. In a control experiment, T_g-based SMCs for uncross-linked TP15 exhibits significant irreversible creep at the higher cycle number of SMCs due to disentanglement of polymeric chain (Figure S5, Supporting Information). Moreover, the lower shape recovery

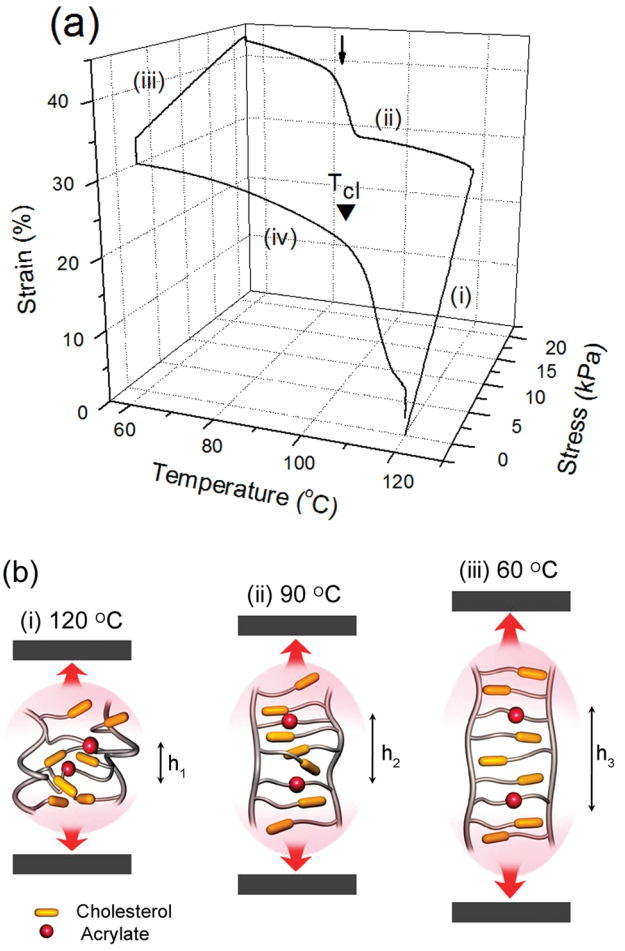

Figure 6. (a) 3D diagram of T_{cl}-based one-way shape memory cycle (1W-SMC, fourth cycle) for XL-TP15, where spontaneous increase of strain is indicated by an arrow: (i) deformation, (ii) cooling, (iii) unloading and shape fixing, and (iv) recovery. (b) Schematic illustration for spontaneous increase of stain when cooling the XL-TP15 under constant force, where constant force direction is indicated by red arrows: (i) XL-TP15, adopting a Gaussian configuration at the isotropic state (120 °C), (ii) initial formation of interdigitated SmA layers at 90 °C, and (iii) complete formation of interdigitated SmA layer at 60 °C. The distance between cross-links (red balls) increases ($h_1 < h_2 < h_3$) by the development of SmA layers when the sample is cooled under constant force applied to a certain direction. This leads to the overall spontaneous increase of strain of the XL-TP15.

during SMCs observed in TP15 compared to XL-TP15 could be attributed to the larger plastic deformation resulting from unconstrained, sliding polymer chains in TP15.

(*ii*). *T_{cl}-Based SMCs*. T_{cl}-based SMCs of XL-TP15 is investigated by monitoring strain responses as a function of temperature (60−120 °C) and stress (2.3−18.7 kPa). Four consecutive SMCs are performed and a representative 3D plot based on the fourth cycle of T_{cl}-based SMCs for XL-TP15 is described in Figure 6a. The temperature range (60−120 °C) is selected to allow evaluation of T_{cl} independently from the T_g-based SMCs (0−60 °C). In the first step (deformation), the sample is uniaxially elongated at the isotropic state (120 °C). The applied stress (18.7 kPa) is approximately five times less than the stress in the T_g-based SMCs due to much lower E' (0.034 MPa) in the isotropic state (120 °C) compared to E' (4.00 MPa) in the LC state (60 °C) as shown in the linear viscoelastic experiment (Figure 3). In the second step (cooling), the sample is cooled to 60 °C under constant stress, and there is a noticeable jump of strain (14.3%) starting at temperature (90 °C) where SmA ordering begins. The

Table 4. Strain, Shape Fixity (R_f), and Shape Recovery (R_r) of XL-TP15 in T_{cl}-Based SMCs[a]

cycle no.	strain (%)	R_f (%)	$R_r(1)$[b] (%)	$R_r(2)$[c] (%)
1	65.5	81.7	78.8	87.2
2	54.1	80.0	82.5	91.5
3	47.9	79.0	84.5	93.4
4	44.0	78.9	85.9	94.5

[a] Conditions during SMCs: Temperature (60−120 °C) and applied stress (18.7 kPa). [b] $R_r(1)$ is a shape recovery at 120 °C. [c] $R_r(2)$ is a shape recovery at 120 °C after 20 min of isothermal step.

spontaneous increase of strain under constant stress is probably due to cooling-induced elongation.[34] Cooling the sample below the isotropic state leads to entropy reduction caused by the ordering of SmA layer along the stretching direction. The development of SmA layers between chemical junctions pushes cross-links apart upon cooling from the isotropic state to the LC state, and thereby spontaneous macroscopic increase of strain is observed along the stretching direction (Figure 6b). In the third step (unloading and shape fixing), the applied load is removed so that the temporary shape is obtained. The temperature is further held for 10 min at 60 °C after removing the stress to ensure shape fixity by the formation of SmA ordering. The removal of stress accompanies strain reduction resulting in relatively poor shape fixing (average $R_f \sim 79.9\%$) compared to the T_g-based SMCs (average $R_f \sim 97.5\%$). However, the strain remains nearly constant during 10 min of isothermal period. This result suggests that shape fixing is enabled by the formation of interdigitated SmA layers rather than vitrification or crystallization. In the fourth step (recovery), the sample recovers the original shape by regaining entropy elasticity when reheated to 120 °C.

Quantitative analysis of the T_{cl}-based SMCs on XL-TP15 is shown in Table 4. The first cycle retains thermomechanical history of the sample during preparation such that relatively large reduction of the strain is observed between first and second cycle when the thermal history is removed. The strain decreases at higher cycle numbers because increased stiffness of the sample induced by the orientation of the sample in stretching direction makes the sample resilient to elongation in following cycles.[64] R_f in the T_{cl}-based SMCs are lower than those in the T_g-based SMCs. This is because the unloading step is carried out at 60 °C, which is still above T_g (22.5 °C) indicating the absence of vitrifcation in the sample. The shape fixing in the T_{cl}-based SMCs is due to the ordering of highly interdigitated SmA layers, however, shape fixing is relatively weaker compared to the T_g-based SMCs. Compared to the T_g-based SMCs, shape recovery in the T_{cl}-based SMCs gets completed within a narrower temperature range due to faster stress-relaxation resulting from dramatic microstructural changes from the LC state to the isotropic state. Also, higher R_r value ($R_r(1) = 85.9\%$, fourth cycle) is obtained as soon as the temperature reaches to 120 °C, and remaining strain is further recovered during additional 20 min of isothermal step at 120 °C ($R_r(2) = 94.5\%$, fourth cycle). The T_{cl}-based SMCs show improvement in R_r with increased cycle number, which has also been reported previously.[26] It is also important to point out that cross-links are important for the T_{cl}-based SMCs. Thermomechanical experiments for TP15 is not feasible since the sample flows in the isotropic state (120 °C) due to lack of cross-links.

(*iii*). *($T_g + T_{cl}$)-Based SMCs*. We investigate the contribution of two different thermal transitions to the shape recovery event by choosing the temperature range as 0−120 °C, which includes both T_g and T_{cl}. Lendlein et al. have shown that if 1W-SMCs (0−70 °C) are programmed to include two

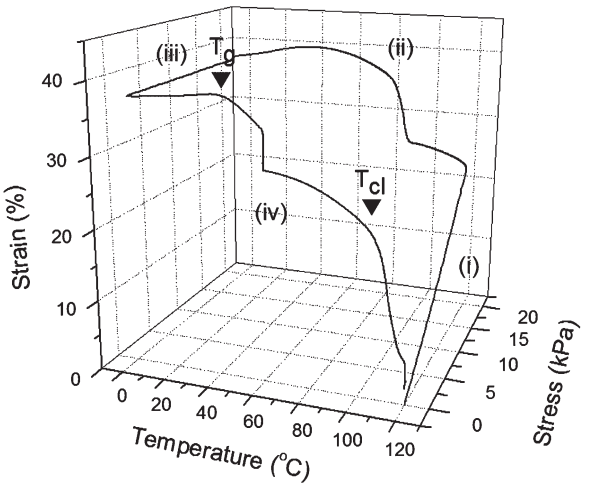

Figure 7. 3D diagram of (T_g+T_{cl})-based one-way shape memory cycle (1W-SMC, 4th cycle) for XL-TP15: (i) deformation, (ii) cooling, (iii) unloading and shape fixing, and (iv) recovery.

independent melting transitions arising from a multicrystallizable phase network based on poly(ethylene glycol) (PEG, T_m ~38 °C) and poly(ε-caprolactone) (PCL, T_m ~54 °C), the shape fixing is dominated by crystallization of PCL. As a result, the shape recovery is not observed at lower melting transition of PEG, but exclusively triggered by higher melting transition of PCL.[65] Additionally, these researchers have demonstrated that the triple shape effect (TSE) is feasible using the polymer networks based on PCL and poly(cyclohexyl methacrylate) (PCHMA).[66] When 1W-SMCs (−10 to + 150 °C) are programmed to include both T_m (~47 °C) of PCL and T_g (~140 °C) of PCHMA, the temporary shape is attained by the contribution of both crystallization of PCL and vitrification of PCHMA. As a result, in the recovery step, the permanent shape is restored in two stages by melting of PCL crystallites and by softening of amorphous PCHMA. This recovery step is similar to the recovery profile of conventional TSE, which requires two deformation steps at different temperature window.[67] Therefore, the purpose of our ($T_g + T_{cl}$)-based SMCs is to determine whether the shape fixing and shape recovery originates from the contribution of vitrification (T_g) and smectic ordering (T_{cl}) or dictated by a particular transition in case of a single phase system, thereby assessing the possibility of TSE.

The ($T_g + T_{cl}$)-based SMCs are conducted by programming cyclic, thermomechanical cycles similar to the T_{cl}-based SMCs. However, temperature range (0−120 °C) includes both T_g (22.5 °C) and T_{cl} (103.5 °C) and the recovery step is divided into two stages. In the first stage of recovery, the sample is first heated from 0 to 60 °C and isothermally held at 60 °C for 20 min, and in the second stage of recovery, the sample is heated from 60 to 120 °C and isothermally held at 120 °C for 20 min. A representative 3D plot of the ($T_g + T_{cl}$)-based SMCs is shown in Figure 7. The strain increases when the stress applied to the sample at the elevated temperature (120 °C), followed by cooling the sample down to 0 °C under constant stress. At this temperature, the temporary shape is obtained by unloading the applied force, and finally, the original shape is restored by reheating the sample in stages to 60 °C and to 120 °C at a constant rate of 3 °C/min.

The overall shape of (T_g+T_{cl})-based SMCs shown in Figure 7 and its quantitative SMCs analyses listed in Table 5 exhibits both characteristics of the T_g and the T_{cl}-based SMCs. In the second step (cooling) of SMCs, cooling-induced elongation at 90 °C is observed similar to the T_{cl}-based

Table 5. Strain, Shape Fixity (R_f), and Shape Recovery (R_r) of XL-TP15 in ($T_g + T_{cl}$)-Based SMCs[a]

cycle no.	strain (%)	R_f (%)	$R_r(1)$[b] (%)	$R_r(2)$[c] (%)	$R_r(T_g)$[d] (%)	$R_r(T_{cl})$[e] (%)
1	62.7	95.3	24.6	85.9	28.6	71.4
2	50.2	94.5	26.4	91.5	28.9	71.1
3	43.9	93.9	27.0	93.6	28.9	71.1
4	40.1	93.4	27.1	94.4	28.7	71.3

[a] Conditions during SMCs: Temperature (60−120 °C) and applied stress (18.9 kPa). [b] $R_r(1)$ is a shape recovery at 60 °C after 20 min of isothermal step. [c] $R_r(2)$ is a shape recovery at 120 °C after 20 min of isothermal step. [d] $R_r(T_g)$ is the contributed percentage of shape recovery triggered only by T_g. [e] $R_r(T_{cl})$ is the contributed percentage of shape recovery triggered only by T_{cl}.

SMCs (Figure 6). In the third step (unloading and shape fixing) of SMCs, the ($T_g + T_{cl}$)-based SMCs exhibits good shape fixity (R_f = 93%, fourth cycle) due to vitrification process similar to the T_g-based SMCs (Figure 5). The strain decreases during first few cycles similar to the T_{cl}-based SMCs due to the increased stiffness by the orientation of the sample under uniaxial elongation. The improved shape recovery profile with higher cycle numbers is analogous to the T_{cl}-based SMCs.

However, there are some differences in the strain response between the T_{cl} and the ($T_g + T_{cl}$)-based SMCs when cooling and reheating the sample. In the ($T_g + T_{cl}$)-based SMCs, the sample contracted 2.7% when cooled below T_g under constant stress due to increase of the E' in the glassy state and thermally expanded by 1.4% under a minimal load (0.01 N) when reheating above T_g. The observed thermal contraction/expansion is probably due to the high coefficient of thermal expansion (CTE) of the XL-TP15. Regardless of the magnitude of strain, the contracted and expanded strain values are similar throughout the SMCs.

Interestingly, the shape recovery event in the ($T_g + T_{cl}$)-based SMCs is triggered by two different temperature windows at T_g and T_{cl}. When the sample is first heated to 60 °C, the temperature between T_g and T_{cl}, the sample only partially recovers its permanent shape ($R_r(1)$ = 27.1%, fourth cycle). The majority of permanent shape is eventually restored after heating the sample to 120 °C ($R_r(2)$ = 94.4%, fourth cycle). The contributed percentage of the shape recovery triggered by T_g and T_{cl} can be independently estimated by calculating ratio between $R_r(1)$ and $R_r(2)$. The contributions from T_g and T_{cl} for the shape recovery events are 28.8% and 71.2%, respectively. These results suggest that the recovery profile of the ($T_g + T_{cl}$)-based SMCs is similar to that of conventional TSE, which usually requires two deformation stages of a sample at two different temperature windows.[67] Therefore, our system can be modified such that we can tailor both the transition temperature range (T_g and T_{cl}) and the percentage recovery at each temperature for shape memory devices remembering multiple-stages of temporary shapes.[24,66−68]

(*iv*). *Comparison of Shape Recovery Events for Different SMCs*. We examine shape recovery events during the T_g, T_{cl}, and ($T_g + T_{cl}$)-based SMCs to elucidate influence of the each transition temperature upon recovery process. Strain and temperature as a function of time during shape recovery in the last cycle of the T_g, T_{cl}, and (T_g+T_{cl})-based SMCs are compared in Figure 8. The shape recovery triggered by T_g is slow since the recovery event occurs through broad range of temperature (25−60 °C) (Figure 8a). The strain does not fully recover even though temperature reaches 60 °C. The average R_r at 60 °C during five consecutive cycles is 60.8%, and the residual strain is finally recovered when the sample is further annealed for 40 min at 60 °C (average $R_r(2)$ = 96%).

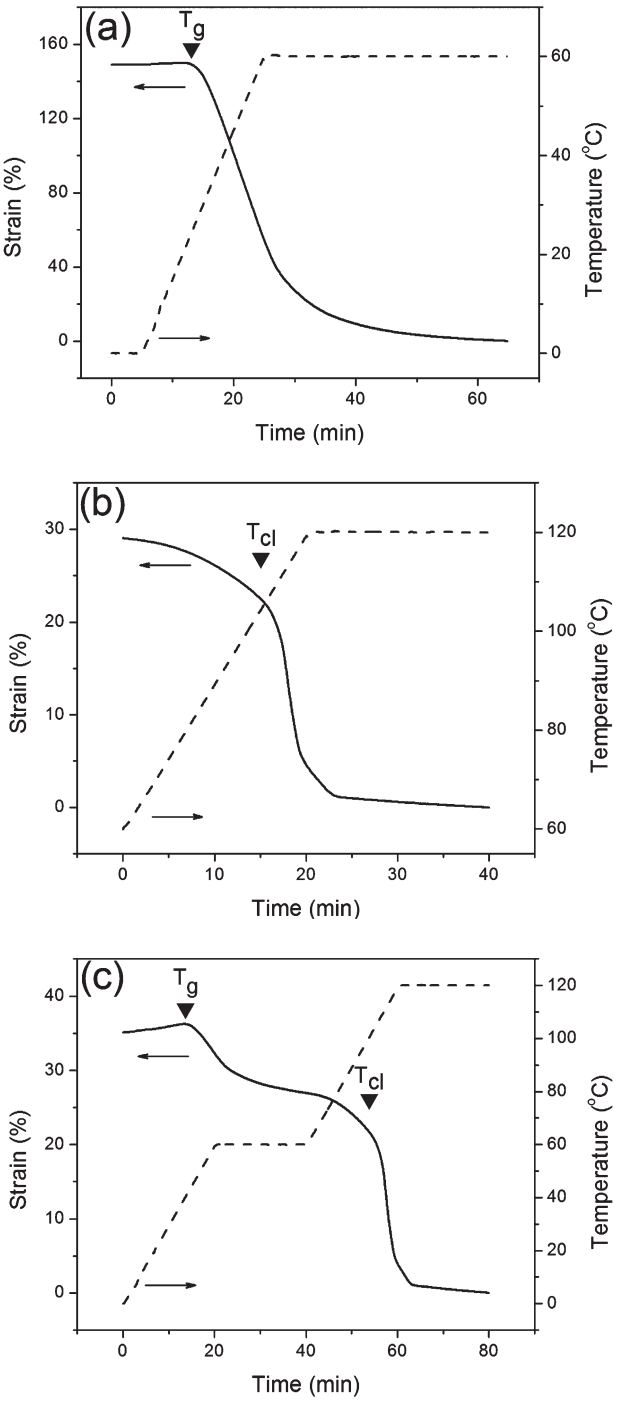

Figure 8. Time vs strain and temperature during shape recovery: (a) T_g-based SMC, (b) T_{cl}-based SMC, and (c) ($T_g + T_{cl}$)-based SMC.

The slow recovery by T_g is attributed to slow relaxation of polymer chain around T_g.[1,63] Meanwhile, the shape recovery triggered by T_{cl} (Figure 8b) is completed within narrower temperature range (105−120 °C). The average R_r at 120 °C during four consecutive cycles is 83.0%, and the residual strain recovers during additional 20 min of isothermal step at 120 °C. The faster shape recovery of the T_{cl}-based SMCs is attributed to dramatic microstructural change from the highly interdigitated SmA phase to the isotropic phase.[1,63]

When both T_g and T_{cl} are used as a T_{trans}, the permanent shape is regained through the two stages of shape recovery (Figure 8c). In other words, the temporary shape is obtained by contribution of both vitrification and formation of ordered SmA layers. During recovery process, the sample starts to regain its permanent shape as the temperature increases beyond T_g, however, the shape recovery event is completed only when the sample is heated back to above T_{cl}. About 28.8% of shape recovery is obtained around T_g and the rest 71.2% of recovery is achieved when the temperature exceeds T_{cl}. Thus, the overall shape recovery event in the (T_g+T_{cl})-based SMCs occurs through much wider temperature range (40−120 °C), and the amount of shape recovery can be controlled by choosing different final temperature.

The temperature where the shape recovery starts is higher in case of ($T_g + T_{cl}$)-based SMCs (~40 °C, Figure 8c) than that of the T_g-based SMCs (~25 °C, Figure 8a). This is attributed to the orientation effect of both vitrified and SmA domains when the sample is deformed at temperature above both T_g and T_{cl} for the ($T_g + T_{cl}$)-based SMCs, while the vitrified domain is mainly oriented for the T_g-based SMCs. As a result, higher thermal energy is required to trigger shape recovery resulting in increased T_g for the ($T_g + T_{cl}$)-based SMCs.

3. Summary

In this article, we describe synthesis and characterization of a side-chain liquid crystalline type random terpolymer (TP15), its cross-linked network (XL-TP15), and its three different 1W-shape memory properties. Analyses on shape memory properties are conducted by DMA by programming three different 1W-SMCs using two different transition temperatures including T_g, T_{cl}, and combination of T_g and T_{cl}: (1) T_g-based SMCs reveal excellent shape memory performance with high shape fixing (>97%), shape recovery ratio (>96%), and large strain (150%), (2) T_{cl}-based SMCs show spontaneous elongation of strain at the temperature where SmA ordering begins, indicating that the development of interdigitated SmA phase is responsible for the observed phenomenon, and (3) ($T_g + T_{cl}$)-based SMCs exhibit the two stages of recovery at T_g and T_{cl}, indicating that XL-TP15 can exhibit triple shape capability.

Currently, we are exploring the influence of extent of interdigitation in SmA layers on the final shape memory properties by varying the flexible methylene spacer length between polymer backbone and cholesteryl side-chains. Moreover, 2W-SME as well as TSE[67] are being investigated using these polymers and this will expand potential applications of these polymers in smart materials, thermal actuators and multiple-stage shape memory devices.[68] Given that numerous ROMP monomers[69−72] can be easily synthesized and some are commercially available, we believe that our synthetic method will allow easy access to polymers with tunable shape memory properties for applications in biomedical devices and thermal actuators.

4. Experimental Section

Materials. 5-Norbornene-2-carboxylic acid (NBCOOH, mixture of *endo* and *exo,* 98%), 4-hydroxybutyl acrylate (4-HBA, 90%), Grubbs catalyst second generation, ethyl vinyl ether (EVE, 99%), oxalyl chloride (98%), anhydrous THF (99.9%), are purchased from Sigma-Aldrich and used without further purification. Poly(ethylene glycol) (average M_w~300 g/mol) and dry CH_2Cl_2 (99.8%) are obtained from Acros Organics.

Synthesis of Poly(ethylene glycol) Functionalized Norbornene (NBPEG). NBCOOH (86.4% *endo* and 13.6% *exo*) (7.0 g, 50.7 mmol) is dissolved in 20 mL of CH_2Cl_2 and purged with nitrogen for 15 min. To this solution, excess oxalyl chloride (17.43 mL, 202.89 mmol) is injected in a dropwise manner, followed by adding a drop of dimethylformamide (DMF). After 12 h reaction at room temperature, unreacted oxalyl chloride is removed under reduced pressure, resulting in norbornene carbonyl chloride (NBCOCl). To the resultant NBCOCl, poly(ethylene glycol)

(M_n = 300 g/mol) (60.9 g, 202.9 mmol) and triethylamine (7 mL, 50.7 mmol) are added, followed by stirring for 18 h under nitrogen at room temperature. The organic phase is washed with 2 M HCl (300 mL). The crude product is initially purified by column chromatography (silica gel, ethyl acetate) until a single spot is observed on a TLC plate. Then, the pure product remaining inside column is finally collected by running methanol (pale yellow liquid, yield 50.0%, *endo*/*exo* = 82/18).

^{1}H NMR (500 MHz, $CDCl_3$, δ): 5.90, 6.15 (m, 2H, cyclic, $-CH{=}CH-$, *endo*), 6.08 (m, 2H, cyclic, $-CH{=}CH-$, *exo*) 4.14, 4.21 (m, 2H, $-COO-CH_2CH_2O-$, *endo*/*exo*), 3.57−3.70 (m, 26H, $-CH_2CH_2O-(CH_2CH_2O)_5-CH_2CH_2-OH$), 2.22−3.18 (m, 3H, cyclic, $-CH-$, *endo*/*exo*), 2.61 (s, 1H, CH_2CH_2-OH), 1.23, 1.49, 1.88 (m, 2H, cyclic, $-CH_2-$, *endo*/*exo*), 1.33−1.38 (m, 2H, cyclic, $-CH_2-$, *endo*/*exo*). ^{13}C NMR (125 MHz, $CDCl_3$, δ): 176.2 (*x*), 174.7 (*n*), 138.1 (*x*), 137.7 (*n*), 135.7 (*x*), 132.4 (*n*), 72.6, 70.6, 70.3, 69.2, 67.9, 63.5 (*x*), 63.3 (*n*), 61.6, 49.6 (*n*), 46.7 (*x*), 46.3 (*x*), 45.7 (*n*), 43.3 (*n*), 43.1 (*x*), 42.5 (*n*), 41.7 (*x*), 30.4 (*x*), 29.2 (*n*). IR (KBr, disk, ν /cm^{-1}): 3353 (−OH st), 3059 (=CH_2 st), 2842−2870 (aliphatic C−H st), 1731 (C=O st), 1110 (C−O st), 714 (=CH δ). ESI−MS: MS data shows mass distribution from 220.9 to 688.7 *m*/*z* with maximum at 512.7. This is accordance with calculated molecular weight for 8 repeating unit of glycol groups [$C_{24}H_{41}$ $O_{10}Na^+$] 512.57. Furthermore, PEG derivatives with 6 (424.7 *m*/*z*), 7 (468.7 *m*/*z*), 9 (556.7 *m*/*z*), and 10 (600.7 *m*/*z*) ethylene glycol repeating units are also found.

Synthesis of 5-(Acryloyl butoxycarbonyl)bicyclo[2.2.1]hept-2-ene (NBBA). NBBA is synthesized and purified according to a modified literature procedure.[60] The crude product is purified by column chromatography (silica gel, ethyl acetate/*n*-hexane = 1/7) resulting in viscous colorless liquid. (Yield 33.4%, *endo*/*exo* = 80/20)

^{1}H NMR (500 MHz, $CDCl_3$, δ): 5.80, 6.38 (dd, 2H, vinylic, $-COO-CH{=}CH_2$), 6.10 (dd, 1H, vinylic $-COO-CH{=}CH_2$), 5.90, 6.17 (m, 2H, cyclic, $-CH{=}CH-$, *endo*), 6.10 (m, 2H, cyclic, $-CH{=}CH-$, *exo*) 4.17 (t, 2H, $-CH_2-CH_2-COO-$), 4.04, 4.10 (m, 2H, $-COO-CH_2-CH_2-$, *endo*/*exo*), 2.20−3.18 (m, 3H, cyclic, $-CH-$, *endo*/*exo*), 1.26, 1.49, 1.88 (m, 2H, cyclic, $-CH_2-$, *endo*/*exo*) 1.73 (m, 4H, $-CH_2-(CH_2)_2-CH_2-$), 1.33−1.41 (m, 2H, cyclic, $-CH_2-$, *endo*/*exo*). ^{13}C NMR (125 MHz, $CDCl_3$, δ): 175.9 (*x*), 174.4 (*n*), 165.9, 137.9 (*x*), 137.6 (*n*), 135.7 (*x*), 132.3 (*n*), 130.1, 128.6, 63.9, 63.7 (*x*), 63.5 (*n*), 49.6 (*n*), 46.6 (*x*), 46.3 (*x*), 45.7 (*n*), 43.4 (*n*), 43.2 (*x*), 42.5 (*n*), 41.6 (*x*), 30.3 (*x*), 29.3 (*n*), 25.5. IR (KBr, disk, ν /cm^{-1}): 3063 (=CH_2 st), 2949−2844 (aliphatic C−H st), 1726 (C=O st), 1622 (C=C st), 1470 ($-CH_2$ δ), 1194 (C−O st), 710 (=CH δ). GC−MS (*m*/*z*): 264 (M), 66 (100). Anal. Calcd for $C_{15}H_{20}O_4$: C, 68.16; H, 7.63. Found: C, 67.77; H, 7.43.

Synthesis of Terpolymer (TP15). NBCh15 (2.00 g, 2.64 mmol), NBPEG (223.5 mg, 0.512 mmol) and NBBA (50.2 mg, 0.19 mmol) are preweighed and dissolved in 30 mL of dry CH_2Cl_2 and purged with nitrogen for 15 min. Similarly, preweighed Grubbs catalyst second generation (15.3 mg, 0.018 mmol) in 5 mL of CH_2Cl_2 is purged with nitrogen for 15 min. The monomers and catalyst solutions are combined together. Polymerization is allowed to proceed for 1.5 h at room temperature under nitrogen and terminated by adding ethyl vinyl ether (EVE, 3.0 mL, 31.3 mmol). The resulting polymer is precipitated in methanol, followed by drying overnight under vacuum at room temperature. (2.05 g, yield 89.4%)

^{1}H NMR (500 MHz, $CDCl_3$, δ): 5.80, 6.38 (dd, 2H, vinylic, $-COO-CH{=}CH_2$), 6.10 (dd, 1H, vinylic $-COO-CH{=}CH_2$), 5.21−5.35 (m, 6H, cyclic, $-CH{=}CH-$ and 1H, olefinic, $=CH-$ in cholesteryl), 4.60 (m, 1H, $-COO-CH-$ in cholesteryl), 4.01−4.16 (m, 8H in methylene spacer), 3.63 (m, 26H, $-CH_2CH_2O-(CH_2CH_2O)_5-CH_2CH_2-OH$).

Instrumental Procedures. ^{1}H NMR and ^{13}C NMR spectra (Bruker DMX 500 MHz NMR spectrometer) are recorded at room temperature with tetramethylsilane (TMS) as an internal standard and deuterated chloroform ($CDCl_3$) as lock solvent. Fourier transform infrared (FT-IR) spectroscopy (Niclotet Magna 560 FTIR spectrometers, transmission mode) is employed to characterize functional groups. Elemental analysis is carried out using a Vario MICRO Elementar, calibrated with sulfanilamide standard, which simultaneously detects C, H, N, and S percentage. Mass spectra are obtained on a Hewlett-Packard 5890 series II gas chromatography−mass spectrometer and a Micromass Quattro-II triple quadrupole mass spectrometer equipped with an electrospray ionization (ESI) positive ion mode source. Gel permeation chromatography (GPC) is carried out to obtain molecular weight and polydispersity indices (PDI) of polymers using a Waters 1515 coupled with a PL-ELS1000 evaporative light scattering (ELS) detector and a Waters 2487 dual wavelength absorbance detector UV−vis detector in THF as eluent with a flow rate of 2.0 mL/min. Samples for GPC are prepared by dissolving THF (~1 mg/mL) for overnight, followed by passing through a 0.45 μm PTFE filter before injection. Polystyrene standards are used for constructing calibration curves. Glass transition temperature (T_g), clearing temperature (T_{cl}) and heat of fusion (ΔH) are determined from differential scanning calorimetry (DSC) by a TA-2920 DSC (Q-100 series) instrument under a nitrogen purge. Calibration is conducted by Indium standard. Temperature range for analysis is typically −50 to +150 °C with scanning rate as 10 °C/min. Sample is preheated to 150 °C to remove thermal history and second heating curves is recorded to determine T_g, T_{cl}, and ΔH using Universal Analysis software.

Curing: Preparation of Polymer Network (XL-TP15) by Cross-Linking Terpolymer (TP15). The terpolymer powder (TP15) is compression molded at 50 °C under air, resulting in an uncross-linked TP15 film with uniform thickness. Then, the film placed between two hot plates is thermally cured inside vacuum oven at 120 °C. During the cross-linking process, a small piece cut from the entire sample is taken out from hot plates periodically to determine gel fraction at different curing time. The gel fraction analysis on cured TP15 is carried out by Soxhlet extraction using THF as extracting solvent for 24 h. The gel fraction values are determined by the ratio between initial mass of XL-TP15 before extraction (m_i) and dried mass of XL-TP15 after extraction (m_d),

$$G\,(\%) = \frac{m_d}{m_i} \times 100$$

Microstructural Analysis. 1-D and 2-D WAXD analyses are conducted to determine the liquid crystalline phase. For 1-D WAXD, a Bruker AXS D5005 powder diffractometer (reflection mode) is employed with Cu Kα radiation (Graphite monochromator, λ = 1.542 Å) generated at 40 kV and 40 mA in the range of $1.4° < 2\theta < 25.0°$. 2-D WAXD is carried out on Oxford Diffraction XCalibur PX Ultra (transmission mode) with Onyx detector in the rage of $2.8° < 2\theta < 51.1°$ (Cu Kα radiation 1.542 Å, double mirror focusing, 40 kV and 40 mA). A film of TP15 (10.0 mm length × 2.0 mm width × 0.7 mm thickness) is prepared by compression molding the powdered sample at 50 °C.

Linear Viscoelastic Properties. Linear viscoelastic properties of the XL-TP15 are measured by a dynamic mechanical analyzer (DMA, TA Instrument DMA 2980) with cryo accessory attached. A tension film mode is employed with a preload force of 0.01 N, a heating rate of 3 °C/min, force tracking of 125%, and an oscillation frequency of 1 Hz. The amplitude is adjusted during the experiment from the initial value of 15 μm to the final value of 250 μm. The sample used for DMA is a rectangular slab of 5.97 mm (length) × 5.55 mm (width) × 0.51 mm (thickness).

Shape Memory Cycles. Cyclic thermomechanical analysis is performed on a DMA (tension film clamp, controlled force mode). The TP15 sample for SMCs is prepared by compression-molding the powder material at 50 °C and the XL-TP15 sample is prepared by curing the TP15 sample at 120 °C under vacuum for 48 h. The prepared films are cut into a rectangular piece of average dimension 6.5 mm (length) × 4.2 mm (width) × 0.7 mm (thickness).

T_g-Based SMCs. The thermomechanical cycle consists of four consecutive steps. The temperature range is set as 0−60 °C for T_g-based SMCs. The rectangular compression-molded sample is heated to 60 °C and held at 60 °C for 30 min to ensure that the sample has reached thermal equilibrium. In step 1, the sample is uniaxially elongated by ramping force from preload 0.01 to 0.25 N at a rate of 0.05 N/min (deformation). In step 2, the sample is cooled at the rate of 3 °C/min to 0 °C to fix the deformed sample under constant force (cooling). In step 3, the force to the sample is unloaded to preload value (0.01 N) at a rate of 0.05 N/min (unloading and shape fixing). In the final step, sample is reheated at the rate of 3 °C/min to 60 °C and held at 60 °C for 40 min to recover any residual strain (recovery). The thermomechanical cycle consisting of four steps is repeated four more times on the same sample.

T_{cl}-Based SMCs. For T_{cl}-based SMCs, the temperature ranges is 60−120 °C where only T_{cl} serves for the shape memory transition temperature. Prior to deformation, the sample is heated to 120 °C and equilibrated for 30 min. In step 1, the sample is uniaxially deformed by ramping force from preload 0.01 to 0.08 N at a rate of 0.05 N/min (deformation). In step 2, the sample is cooled at the rate of 3 °C/min to 60 °C to fix the deformed sample under constant force (cooling). In step 3, the force to the sample is unloaded to preload value (0.01 N) at a rate of 0.05 N/min. After unloading step, additional 10 min of isothermal step is included to ensure shape fixing by SmA phase at 60 °C (unloading and shape fixing). In the final step, sample is reheated at the rate of 3 °C/min to 120 °C and held at 120 °C for 20 min to recover any residual strain (recovery). The thermomechanical cycle consisting of four steps is repeated three more times on the same sample.

(T_g+T_{cl})-Based SMCs. (T_g+T_{cl})-based SMCs of which temperature range 0−120 °C are similar to the T_{cl}-based SMCs. However, the recovery of strain (step 4) is programmed by increasing temperature with two steps. First, the sample is heated from 0 to 60 °C and held at 60 °C for 20 min to estimate recovery triggered by T_g. Finally, the sample is heated to 120 °C and held for 20 min to assess recovery activated by T_{cl}.

Acknowledgment. Financial support was provided by the University of Connecticut new-faculty start up fund, University of Connecticut Research Foundation faculty grant, and NSF CAREER Award to RMK (DMR-0748398). Central instrumentation facilities in the Institute of Materials Science and Chemistry Department at the University of Connecticut are acknowledged. The authors thank Dr. Haihu Qin (Lubrizol Corp.) and Shih-Po Sun for their helpful discussions and Jaewoo Jang (Honda Motor Co.) for improving quality of illustrations in this publication.

Supporting Information Available: Figures showing ^{1}H NMR of NBPEG and NBBA and a mass spectrum of NBPEG, a table of thermal properties of terpolymers (TP15) with different compositions, a figure showing an energy minimized bilayer model, and a table and figure showing controlled experiments for T_g-based shape memory cycles (SMCs) with uncross-linked TP15. This material is available free of charge via the Internet at http://pubs.acs.org.

References and Notes

(1) Liu, C.; Qin, H.; Mather, P. T. *J. Mater. Chem.* **2007**, *17*, 1543–1558.
(2) Behl, M.; Lendlein, A. *Soft Matter* **2007**, *3*, 58–67.
(3) Behl, M.; Lendlein, A. *Mater. Today* **2007**, *10*, 20–28.
(4) Lendlein, A.; Kelch, S. *Angew. Chem., Int. Ed.* **2002**, *41*, 2034–2057.
(5) Mather, P. T.; Luo, X.; Rousseau, I. A. *Annu. Rev. Mater. Res.* **2009**, *39*, 445–471.
(6) Ahn, S.-k.; Kasi, R. M.; Kim, S.-C.; Sharma, N.; Zhou, Y. *Soft Matter* **2008**, *4*, 1151–1157.
(7) Jiang, H.; Kelch, S.; Lendlein, A. *Adv. Mater.* **2006**, *18*, 1471–1475.
(8) Lendlein, A.; Jiang, H.; Juenger, O.; Langer, R. *Nature* **2005**, *434*, 879–882.
(9) Hribar, K. C.; Metter, R. B.; Ifkovits, J. L.; Troxler, T.; Burdick, J. A. *Small* **2009**, *5*, 1830–1834.
(10) Koerner, H.; Price, G.; Pearce, N. A.; Alexander, M.; Vaia, R. A. *Nat. Mater.* **2004**, *3*, 115–120.
(11) Osada, Y.; Gong, J.-P. *Adv. Mater.* **1998**, *10*, 827–837.
(12) Huang, W. M.; Yang, B.; An, L.; Li, C.; Chan, Y. S. *Appl. Phys. Lett.* **2005**, *86*, 114105.
(13) Mohr, R.; Kratz, K.; Weigel, T.; Lucka-Gabor, M.; Moneke, M.; Lendlein, A. *Proc. Natl. Acad. Sci. U.S.A.* **2006**, *103*, 3540–3545.
(14) Sokolowski, W.; Metcalfe, A.; Hayashi, S.; Yahia, L. H.; Raymond, J. *Biomed. Mater.* **2007**, *2*, S23–S27.
(15) Metcalfe, A.; Desfaits, A.-C.; Salazkin, I.; Yahia, L. H.; Sokolowski Witold, M.; Raymond, J. *Biomaterials* **2003**, *24*, 491–497.
(16) Lendlein, A.; Langer, R. *Science* **2002**, *296*, 1673–1676.
(17) Yakacki Christopher, M.; Shandas, R.; Lanning, C.; Rech, B.; Eckstein, A.; Gall, K. *Biomaterials* **2007**, *28*, 2255–2263.
(18) Neffe, A. T.; Hanh, B. D.; Steuer, S.; Lendlein, A. *Adv. Mater.* **2009**, *21*, 3394–3398.
(19) Wischke, C.; Neffe, A. T.; Steuer, S.; Lendlein, A. *J. Controlled Release* **2009**, *138*, 243–250.
(20) Nagahama, K.; Ueda, Y.; Ouchi, T.; Ohya, Y. *Biomacromolecules* **2009**, *10*, 1789–1794.
(21) Neuss, S.; Blomenkamp, I.; Stainforth, R.; Boltersdorf, D.; Jansen, M.; Butz, N.; Perez-Bouza, A.; Knuechel, R. *Biomaterials* **2009**, *30*, 1697–1705.
(22) Migneco, F.; Huang, Y.-C.; Birla, R. K.; Hollister, S. J. *Biomaterials* **2009**, *30*, 6479–6484.
(23) Mondal, S.; Hu, J. L. *Indian J. Fibre Text. Res.* **2006**, *31*, 66–71.
(24) Bellin, I.; Kelch, S.; Langer, R.; Lendlein, A. *Proc. Natl. Acad. Sci. U.S.A.* **2006**, *103*, 18043–18047.
(25) Kunzelman, J.; Chung, T.; Mather, P. T.; Weder, C. *J. Mater. Chem.* **2008**, *18*, 1082–1086.
(26) Burke, K. A.; Mather, P. T. *J. Mater. Chem.* **2010**, *20*, 3449–3457.
(27) Bertmer, M.; Buda, A.; Blomenkamp-Hoefges, I.; Kelch, S.; Lendlein, A. *Macromolecules* **2005**, *38*, 3793–3799.
(28) Xie, T.; Rousseau, I. A. *Polymer* **2009**, *50*, 1852–1856.
(29) Yakacki, C. M.; Shandas, R.; Safranski, D.; Ortega, A. M.; Sassaman, K.; Gall, K. *Adv. Funct. Mater.* **2008**, *18*, 2428–2435.
(30) Miaudet, P.; Derre, A.; Maugey, M.; Zakri, C.; Piccione, P. M.; Inoubli, R.; Poulin, P. *Science* **2007**, *318*, 1294–1296.
(31) Sakurai, K.; Takahashi, T. *J. Appl. Polym. Sci.* **1989**, *38*, 1191–1194.
(32) Jeon, H. G.; Mather, P. T.; Haddad, T. S. *Polym. Int.* **2000**, *49*, 453–457.
(33) Lee, K. M.; Knight, P. T.; Chung, T.; Mather, P. T. *Macromolecules* **2008**, *41*, 4730–4738.
(34) Chung, T.; Romo-Uribe, A.; Mather, P. T. *Macromolecules* **2008**, *41*, 184–192.
(35) Liu, C.; Chun, S. B.; Mather, P. T.; Zheng, L.; Haley, E. H.; Coughlin, E. B. *Macromolecules* **2002**, *35*, 9868–9874.
(36) Qin, H.; Mather, P. T. *Macromolecules* **2009**, *42*, 273–280.
(37) Rousseau, I. A.; Mather, P. T. *J. Am. Chem. Soc.* **2003**, *125*, 15300–15301.
(38) Weiss, R. A.; Izzo, E.; Mandelbaum, S. *Macromolecules* **2008**, *41*, 2978–2980.
(39) Rubinstein, M.; Colby, R. H., *Polymer Physics*; Oxford University: New York, 2003.
(40) Ahir, S. V.; Tajbakhsh, A. R.; Terentjev, E. M. *Adv. Funct. Mater.* **2006**, *16*, 556–560.
(41) Hiraoka, K.; Sagano, W.; Nose, T.; Finkelmann, H. *Macromolecules* **2005**, *38*, 7352–7357.
(42) Mirfakhrai, T.; Madden, J. D. W.; Baughman, R. H. *Mater. Today* **2007**, *10*, 30–38.
(43) Li, M.-H.; Keller, P. *Philos. Trans. R. Soc., A* **2006**, *364*, 2763–2777.
(44) Xie, P.; Zhang, R. *J. Mater. Chem.* **2005**, *15*, 2529–2550.
(45) Li, M.-H.; Keller, P.; Yang, J.; Albouy, P.-A. *Adv. Mater.* **2004**, *16*, 1922–1925.
(46) Thomsen, D. L.; Keller, P.; Naciri, J.; Pink, R.; Jeon, H.; Shenoy, D.; Ratna, B. R. *Macromolecules* **2001**, *34*, 5868–5875.
(47) Naciri, J.; Srinivasan, A.; Jeon, H.; Nikolov, N.; Keller, P.; Ratna, B. R. *Macromolecules* **2003**, *36*, 8499–8505.
(48) Nishikawa, E.; Finkelmann, H. *Macromol. Chem. Phys.* **1997**, *198*, 2531–2549.
(49) Ahn, S.-K.; Nguyen Le, L. T.; Kasi, R. M. *J. Polym. Sci., Part A: Polym. Chem.* **2009**, *47*, 2690–2701.
(50) Wu, S. K.; Rabek, J. F. *Polym. Degrad. Stab.* **1988**, *21*, 365–376.

(51) Nishikawa, E.; Finkelmann, H.; Brand, H. R. *Macromol. Rapid Commun*. **1997**, *18*, 65–71.
(52) Williams, R. M.; Chapman, D. *Prog. Chem. Fats Other Lipids* **1970**, *11*, 1–79.
(53) Stendahl, J. C.; Li, L.; Claussen, R. C.; Stupp, S. I. *Biomaterials* **2004**, *25*, 5847–5856.
(54) Simons, K.; Ikonen, E. *Science* **2000**, *290*, 1721–1726.
(55) Gopalakrishna, P.; Chaubey, S. K.; Manogaran, P. S.; Pande, G. *J. Cell. Biochem*. **2000**, *77*, 517–528.
(56) Smith, D.; Pentzer, E. B.; Nguyen, S. T. *Polym. Rev*. **2007**, *47*, 419–459.
(57) Zalipsky, S. *Adv. Drug Delivery Rev*. **1995**, *16*, 157–182.
(58) Bertin, P. A.; Watson, K. J.; Nguyen, S. T. *Macromolecules* **2004**, *37*, 8364–8372.
(59) Alfred, S. F.; Al-Badri, Z. M.; Madkour, A. E.; Lienkamp, K.; Tew, G. N. *J Polym. Sci., Part A: Polym. Chem*. **2008**, *46*, 2640–2648.
(60) Liaw, D.-J.; Huang, C.-C.; Hong, S.-M.; Chen, W.-H.; Lee, K.-R.; Lai, J.-Y. *Polymer* **2006**, *47*, 4613–4621.
(61) Quan, C.; Soroush, M.; Grady, M. C.; Hansen, J. E.; Simonsick, W. J. *Macromolecules* **2005**, *38*, 7619–7628.
(62) Grady, M. C.; Quan, C.; Soroush, M. US Patent 20050003094 A1, 2005.
(63) Rousseau, I. A. *Polym. Eng. Sci*. **2008**, *48*, 2075–2089.
(64) Knight, P. T.; Lee, K. M.; Chung, T.; Mather, P. T. *Macromolecules* **2009**, *42*, 6596–6605.
(65) Bellin, I.; Kelch, S.; Lendlein, A. *J. Mater. Chem*. **2007**, *17*, 2885–2891.
(66) Behl, M.; Bellin, I.; Kelch, S.; Wagermaier, W.; Lendlein, A. *Adv. Funct. Mater*. **2009**, *19*, 102–108.
(67) Behl, M.; Lendlein, A. *J. Mater. Chem*. **2010**, *20*, 3335–3345.
(68) Xie, T. *Nature* **2010**, *464*, 267–270.
(69) Pugh, C.; Kiste, A. L. *Prog. Polym. Sci*. **1997**, *22*, 601–691.
(70) Trimmel, G.; Riegler, S.; Fuchs, G.; Slugovc, C.; Stelzer, F. *Adv. Polym. Sci*. **2005**, *176*, 43–87.
(71) Slugovc, C. *Macromol. Rapid Commun*. **2004**, *25*, 1283–1297.
(72) Bielawski, C. W.; Grubbs, R. H. *Prog. Polym. Sci*. **2007**, *32*, 1–29.